Pacific
Northwest
NATIONAL LABORATORY

PNNL-33480

Development of High-Temperature Emissivity Measurement Capabilities for Molten Salts at PNNL

September 2022

Jason M Lonergan
Charmayne E Lonergan

DISCLAIMER

This report was prepared as an account of work sponsored by an agency of the United States Government. Neither the United States Government nor any agency thereof, nor Battelle Memorial Institute, nor any of their employees, **makes any warranty, express or implied, or assumes any legal liability or responsibility for the accuracy, completeness, or usefulness of any information, apparatus, product, or process disclosed, or represents that its use would not infringe privately owned rights**. Reference herein to any specific commercial product, process, or service by trade name, trademark, manufacturer, or otherwise does not necessarily constitute or imply its endorsement, recommendation, or favoring by the United States Government or any agency thereof, or Battelle Memorial Institute. The views and opinions of authors expressed herein do not necessarily state or reflect those of the United States Government or any agency thereof.

Development of High-Temperature Emissivity Measurement Capabilities for Molten Salts at PNNL

September 2022

Jason M Lonergan
Charmayne E Lonergan

Pacific Northwest National Laboratory
Richland, Washington 99354

Abstract

In FY22, PNNL was tasked with the development of an emissivity measurement capability. Emissivity measurements are important for a larger effort to understand radiative heat transfer within molten salts at elevated temperatures (600-1000 °C). Literature review of optical salt properties and radiative heat transfer models indicated that systems within elevated temperature regimes could see upwards of 20% or more of their total heat transferred through photonic mechanisms. Ultimately, future work will measure the total thermal conductivity and break down the molecular and radiative portions. Thermal conductivity, along with other thermal properties of molten salts, both coolant and fuel, are fundamental to modeling and simulations that support molten salt reactor (MSR) design. The results presented here, and ongoing work at PNNL, will be useful in selecting optimal salt compositions, designing reactor systems, and optimizing heat transfer within a MSR power plant.

The initial emissivity measurement concept for a liquid molten salt was developed on the bases of the Stefan-Boltzmann Law. A prototype device operating in ambient atmosphere was constructed and initial results compared well with available literature. The emissivity values for several compositions in the NaCl-KCl system (100% NaCl, 51% NaCl – 49% KCl, and 100% KCl [in mol%]) were measured from 550 to 850 °C and compositions in the NaF-LiF system (NaF, 31mol% NaF – 61mol% LiF, and LiF) were measured from 600 to 1000 °C at a wavelength of 1.3 µm. The NaCl-KCl system appears to be relatively invariant with composition but a clear trend of decreasing emissivity values from ~0.9 at 550 °C to 0.77 at 850 °C was observed. The NaF-LiF system exhibited much clearer compositional dependence, a maximum variance of 0.030 was measured between pure NaF and LiF at 600 °C, but relatively less variation with temperature.

A schematic for an enclosed system for inert atmosphere and actinide salts was drafted. Several of the components for fabrication of this device, improved pyrometer, furnace, nickel for capsule construction, have been purchased and are ready for assembly. The new pyrometer will have an improved measurement range of 275-1000 °C. The clam shell furnace has a maximum temperature of 1200 °C and will support the hermetically sealed inert encapsulation vessels. Nickel plate and tubing will create a relatively corrosion resistance capsule for testing that can withstand temperature up to the 1000 °C maximum measurement temperature of the laser system.

Acknowledgments

Acronyms and Abbreviations

α	Absorptivity
$\hat{\alpha}$	Absorption coefficient
C_p	Heat capacity
D	Thermal diffusivity
ε	Emissivity
H	Enthalpy
HX	Heat exchangers
k	Thermal conductivity
m.p.	Melting point
MSR	Molten salt reactors
MSTDB	Molten Salt Thermal Properties Database
η	Viscosity
NRC	(US) Nuclear Regulatory Commission
ρ	Density
P_{vap}	Vapor pressure
k_e	Effective heat transfer
k_m	Molecular thermal conductivity
k_r	Radiative heat transfer
KF	Karl Fischer
k_t	Total thermal conductivity
R	Reflectance
XRD	X-ray diffraction

Contents

Figures

Tables

1. Introduction

1.1.   Molten Salt Reactors

The International Generation-IV Initiative (GIF) was established in 2001 with the aim of fostering the research and development needed for commercial deployment of generation IV nuclear reactors by 2030.[1, 2] The GIF identified molten salt reactors (MSR) as one of six of the most promising advanced nuclear reactor systems [3-5] With only ~20% of the electricity in the United States coming from nuclear, and a smaller percentage (~10%) for the world, MSR have the potential to overcome the public reluctance of commercial nuclear power with significantly improved safety features and reduced greenhouse emissions.[1, 6, 7]

Origins of the MSR date back to the 1950s with the Aircraft Reactor Experiment project and 1960s with the Molten Salt Reactor Experiment, which were motivated by desires for compact, safer, and more reliable reactors than were available at the time.[8-10] MSR have received growing interest in the nuclear community due to their ability to operate at higher temperatures and to remove the limitations of solid fuels and traditional coolants.[1, 3-5, 11, 12] For instance, present nuclear power plants typically have thermal efficiencies ranging from 34-40%, whereas Brayton-cycle models for MSR running the turbine inlet temperatures at 600°C and 800°C predict efficiencies of 44% and 54% respectively.[13, 14] Many countries have current research projects working to refine and develop this technology for commercial applications, including Japan, France, China, Russia, and the United Kingdom.[11, 15] MSR offer several benefits relative to current light water reactors, including that they are inherently safer, more effectively use actinide fuel, generate less long-lived high-level waste, and do not need solid fuel fabrication.[16-19]. Even considering the benefits of these systems, deployment of the technology has been hindered, partially due to a need for further research and development, particularly related to fuel and coolant materials.

One of the critical materials for MSR is, of course, the molten salt. Salts can be used as a coolant and fuel and a variety of chemistries are of interest. Potential salt chemistries are typically constructed of a mixed binary compound based around a fluoride- or chloride anion bonded to alkali-metal cations such as Li, Be, Na, Mg, and actinides such as Th, Pu, and U. Proposed salt systems are typically comprised of two or more binary salt compounds, taking advantage of eutectic wells to reduce melting temperature. As stated in a US Nuclear Regulatory Commission's (NRC) 2018 report:[20]

> *"Based on earlier studies of MSRs, it is well established that changing the composition of salt can affect properties such as melting point, boiling point, density, and viscosity. Understanding the impact of changes in the thermophysical properties of the fuel/coolant resulting from the addition of fission products and possible corrosion product impurities will be essential to the analyses of the ability to remove heat from the fuel during normal and off-normal conditions and after shutdown."*

Molten salts have numerous technological advantages over current solid fuels and liquid coolants due to their thermophysical properties such as high heat capacity, high boiling point, low vapor pressure, and radiochemical stability.[21-24] They have other beneficial properties such as low viscosities, high ionic conductivity, high power density, and high actinide solubility.[25-33] As they will be used for fuel and coolant materials, it is critical to understand the properties that impact heat transfer and reactor operation.

1.2. Thermal Properties of Salts

Quality, high accuracy measurements of thermal properties of both fuel and coolant salts are essential for modeling and simulation that supports the development and realization of both test and commercial MSR. Of particular interest are measurements at temperatures relevant to normal reactor operation as well as potential off-normal conditions. The effort described here is part of a larger exercise to generate property measurements relevant to industry needs which will result in the development of a Molten Salt Thermal Properties Database (MSTDB).[34] Thermophysical properties that are essential for the successful demonstration of MSR include:

- density (ρ),
- viscosity (η),
- emissivity (ε),
- heat capacity (C_p),
- various enthalpies (H),
- melting point (m.p.),
- vapor pressure (P_{vap}), and
- thermal conductivity (k)

These properties are important to understand, particularly with changing chemistry, as they control the achievable and/or sustainable operational temperatures, radionuclide retention, heat transfer, fissile material carrying capacity, and more. Once measured, these properties will feed into the MSTDB and ultimately be used to aid material selection, reactor development, and commissioning efforts for MSR.

Many single component salts are well understood and have an almost complete set of measurements for the list of properties above. As can be seen in Table 1, some thermal properties are also well studied for many of the eutectic compositions. For example, density and melting temperature are known for many unary, binary, and ternary salt systems as well as some actinide-based salts. It should be noted that Table 1 is a compilation of a portion of relevant chloride coolant salt literature data available and not an exhaustive list of all Cl or F compositions of interest.

Table 1: Summary of several thermophysical properties for various salts.

Molten Salt	ρ (kg/m^3)	m.p. (K)	k_t (W/m·K)	C_p (J/kg·K)	η (pa·s)	P_{vap} (kPa)	ε	Reference
NaCl	✓	✓	✓	✓	✓	✓	✗	[35-38]
KCl	✓	✓	✓	✓	✓	✓	✗	[35-38]
LiCl	✓	✓	✓	✓	✗	✓	✗	[35-38]
MgCl$_2$	✓	✓	✓	✓	✓	✓	✗	[35, 38-40]
NaCl-KCl (eutectic)	✓	✓	✗	✓	✗	✗	✗	[35, 38-43]
NaCl-LiCl (eutectic)	✓	✓	✗	✓	✓	✗	✗	[39, 44]
NaCl-MgCl$_2$ (eutectic)	✓	✓	✓	✓	✓	✓	✗	[38, 39, 45]
KCl-MgCl$_2$ (eutectic)	✓	✓	✓	✓	✓	✓	✗	[38, 39, 45]
LiCl-KCl (eutectic)	✓	✓	✓	✓	✓	✓	✗	[38, 39, 45]
NaCl-KCl-MgCl$_2$ (eutectic)	✗	✓	✗	✓	✗	✗	✗	[45, 46]
NaCl-KCl-LiCl (eutectic)	✓	✓	✗	✗	✗	✗	✗	[45]

While work has been done to understand many properties, there are still wide gaps in the thermophysical property knowledge and weak, unverified data published for binary and ternary compositions. The nearly complete list of measured properties in Table 1 may at first seem like an indication of a job nearly done, but upon closer inspection, it is merely the beginning of what will be necessary to truly understand the intrinsic properties of molten salts. For instance, most of the literature values available have little to no associated measurements of contamination or impurities such as H_2O, OH, or O_2, which are important values to quantify for what are often highly hygroscopic materials. Oxygen and water are known to have significant impacts on behavior such as corrosion and chemical stability, and a deeper understanding of their effects on thermophysical properties are required as well.[20, 34] Thermal conductivity, heat capacity, viscosity, and emissivity all have need for further study.

Although molten salts are often lauded for their low vapor pressures in the liquid state, it is not appropriate to assume volatilization does not occur. A deeper understanding of volatility (whether it's homogeneous or heterogeneous in mixed salts systems) and the change in thermophysical properties with changing compositions is needed. MSR will involve constantly changing chemistries due to volatility, fission products, corrosion products, salt cleaning, and other chemical mechanisms, so it is vitally important to understand the effects of the thermophysical properties outside of pristine eutectic compositions. This is doubly important as most proposed salt systems take advantage of deep eutectic wells to gain access to low melting temperatures (Figure 1, with eutectic well emphasized in 1a and 1b with an arrow).[47] These same eutectic wells could lead to rapid change in properties for off-stoichiometric compositions, as it wouldn't take much of a change in composition or temperature before solid NaCl or $U(Pu)Cl_3$ could crash out of the system.
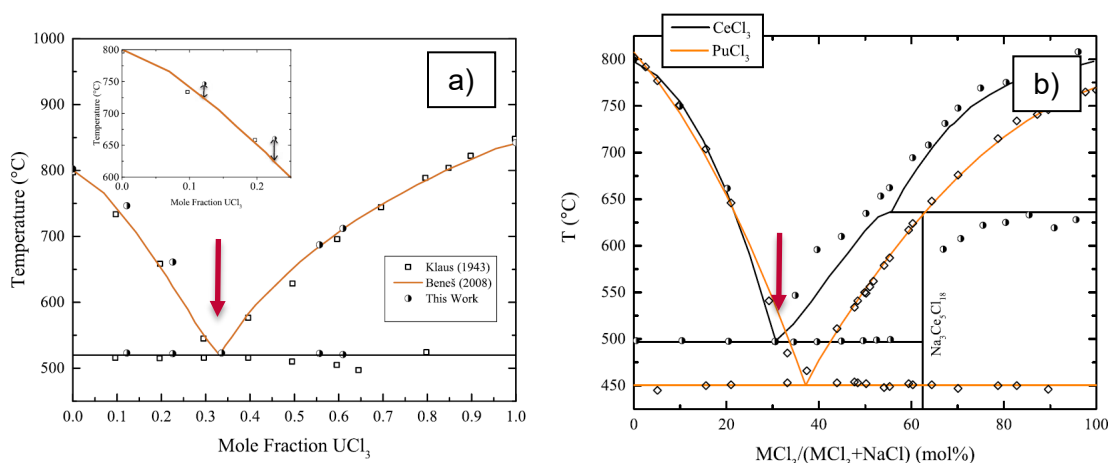
Figure 1. Phase diagrams from E.S. Scooby et al. of the a) $NaCl-UCl_3$ and b) $NaCl-PuCl_3$ systems demonstrating the deep eutectic wells.[47] Arrow indicates $NaCl-UCl_3$ eutectic region.

1.3. Radiative Heat Transfer

In general terms, the power that is produced by a reactor is impacted by the energy flux out of the core.[48] The reactor power may be defined as the core average power density times the core volume. The temperature and pressure that are tolerable by the fuel, coolant, and reactor components determine the achievable power density. Efficient transfer of this power into electricity requires exact knowledge of all the heat transfer processes within the nuclear power plant. Thermal properties are key to determining the operation temperatures of a system, understanding how heat moves through that system, as well as the effectiveness of system

components such as heat exchangers or other parts. Proposed operating temperatures of MSR are at least double that of current generation pressurized water reactors (300 °C versus 600 °C).[49] MSR are slated to operate in a thermal regime where radiative heat transfer may play a significant role. This means that measuring radiative heat transfer properties of the salts are required to accurately predict and model heat transfer within these reactor systems.

Heat transfer can occur by thermal conduction (which includes convection) or thermal radiation.[50] Convection is how heat transfers from a moving fluid to a solid object and is the main mechanism of transfer in a heat exchanger (HX). While conduction is the transmission of heat through static materials such as a wall. Both thermal conduction and convection are energy transport phenomena controlled by the motion of atoms and electrons. Thermal radiation is heat transport resulting from the exchange of electromagnetic waves between two surfaces. This process may occur without another medium present as it dictates the way materials emit thermal energy. Heat transfer within a system or material can involve one or both mechanisms. The heat flux of radiation scales with temperature to the fourth power so is often negligible, relative to conduction, at lower temperatures but becomes more significant as temperatures increase. Assuming heat is radiated homogeneously in all directions from the HXtube, a simple derivation of heat transfer between parallel plates can be determined by considering both mechanisms.[51] The following derivation is a two dimensional cross section in which total heat transfer would be calculated by integrating 360° along the length of the tube axis using polar coordinates. Therefore, the total two-dimensional heat transfer can be given as

$$q_t = q_m + q_{r,x \to y} - q_{r,y \to x} \tag{1}$$

where q_t is the total heat transfer, q_m is the heat transferred by molecular conduction, and $q_{r,x(y) \to y(x)}$ is the radiative heat transfer between two plates (x and y). Note that radiative heat transfer is calculated in both directions, unlike conductivity, which is generally a single mechanism transferring heat from a high temperature area to lower temperature area. According to Ewing et al., the radiative heat flow from one plate to another plate could be reasonably approximated by

$$q_{r,x \to y} = \varepsilon_x A_x \sigma T_x^4 e^{-\hat{\alpha}(\Delta z)} \tag{2}$$

Where, for x plate, ε is emissivity of the tube walls, A is the surface area, and T is the temperature. Additionally, σ is the Stephan-Boltzmann constant, $\hat{\alpha}$ is the absorption coefficient of the salt (which indicates how well the material absorbs light/energy), and Δz is the thickness of the liquid between the plates. Heat transfer by molecular conduction through the salt is derived as

$$q_m = k_m A \frac{T_x - T_y}{\Delta z} \tag{3}$$

where k_m is the thermal conductivity of the molten salt. Assuming the tube walls are black bodies, $\varepsilon = 1$, and dividing through by area and thermal gradient, gives us an expression for effective thermal conductivity (equation 4).[51, 52]

$$k_e = \frac{q_e}{A} \frac{\Delta z}{\Delta T} = k_m + \left(e^{-\hat{\alpha}\Delta z}\right) \frac{\Delta z \sigma \left(T_1^4 - T_2^4\right)}{\Delta T} \tag{4}$$

In equation 4, the effective radiation is highly dependent on three factors, the absorption coefficient, the thickness of the liquid salt, and the temperature. The first two factors scale exponentially and the temperature scales by the fourth power.

It should be noted that the absorptivity and emissivity (which is the ultimate focus of this report) of a body are equivalent when there is thermodynamic equilibrium based on Kirchhoff's Law (Equation 5).[50]

$$\alpha_\lambda = \varepsilon_\lambda \qquad (5)$$

Where α_λ is the wavelength dependent absorptivity of the material, which describes its ability to absorb energy, and ε_λ is the emissivity, which describes a materials ability to emit energy. The absorption coefficient, $\hat{\alpha}$, is a measurement of how far light can go through a material before its absorbed. This value can be calculated from the measurement of emissivity/absorptivity with knowledge of the thickness of the material in question, as shown in Equation 6.

$$\hat{\alpha} = -\frac{ln(1-\alpha_\lambda)}{\Delta z} \qquad (6)$$

To further elucidate the importance of thermal radiation and associated optical properties, the following section will detail the percentage of radiative heat transfer, out of the total heat transfer, using Equations 1-6. Chaleff built a simulation model for HX in which the pipe diameter, operational temperature, and absorption coefficient could be altered.[52] Based on a MSR operation temperature of 800 °C, using experimental values of 5 m^{-1} for the absorption coefficient of FLiNaK(LiF-NaF-KF) salt, and assuming a 2 cm diameter tube, it was estimated that thermal radiation can contribute at least 10% of the total energy transfer for the HX.[52] This model indicated radiation would comprise 15% of the total heat transfer if the operation temperature were increased to 1000 °C. In addition, the measured value for the absorption coefficient of FLiNaK in this study was not known with certainty, and thus may represent a minimum. For example, an increase from 5 to 10 cm^{-1} could easily push the contribution of the radiation portion upwards of 20%. Along with obtaining a complete picture of energy transfer in a system with a HX, thermal radiation is important to understanding how much energy a system absorbs and emits, which can substantially contribute to other heat losses within the reactor. This demonstrates that thermal radiation can significantly contribute to heat transfer and the overall efficiency of a HX and, therefore, the efficiency of MSR.

1.4.   Emissivity

Radiation of energy from a material at any wavelength is dictated by the emissivity. The emissivity of a substance is described relative to an ideal blackbody, i.e. a material where the radiation emitted is equal to that absorbed. In almost every case, the emitted radiation of a real material is less than that emitted by an ideal blackbody at the same temperature.[53] Energy versus wavelength for an ideal blackbody and an unknown object is shown below for comparison (Figure 2). According to Kirchoff's law, the emissivity is equal to the material's absorptivity, assuming thermal equilibrium. Thus, emissivity can also be derived from two other optical properties, transmittance and reflectance.
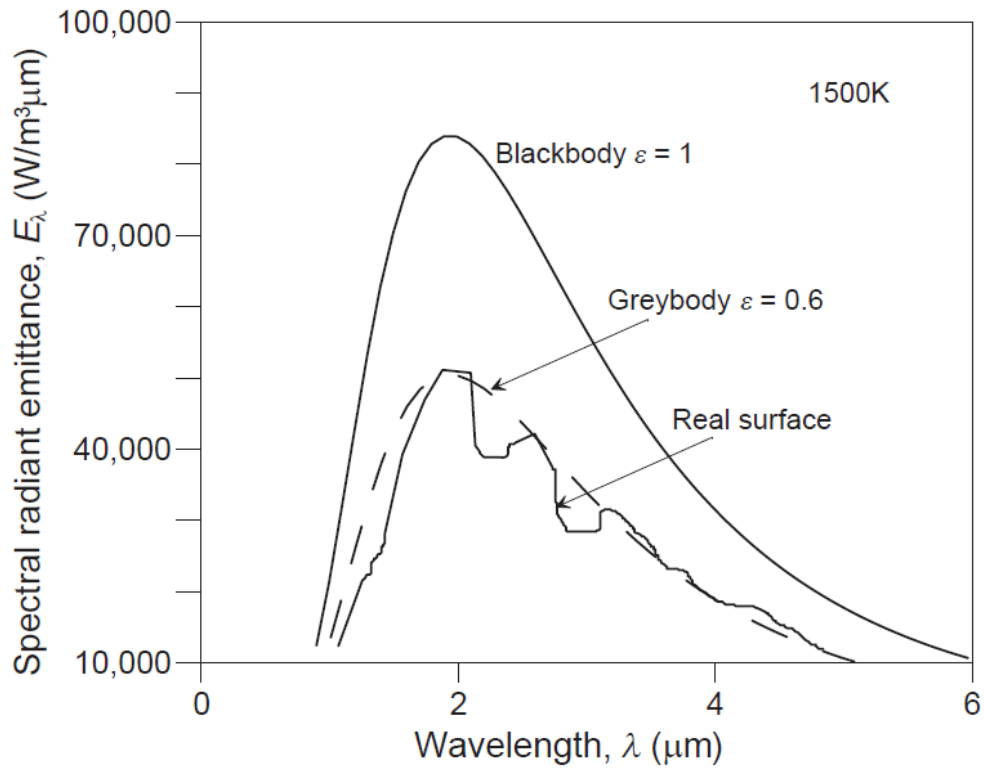
Figure 2. Energy vs. wavelength for an ideal blackbody relative to a gray body and a non-ideal (real) emitter.[54]

Depending on the surface characteristics of the material, electromagnetic waves will either be reflected, transmitted, absorbed, or some combination of the three when they hit a given surface. Below is a graphic (Figure 3) that shows all three interactions.
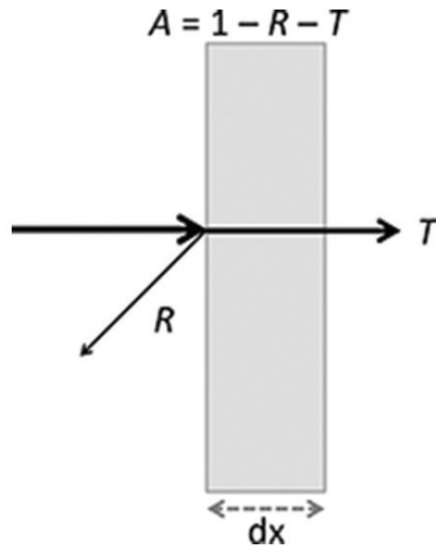
Figure 3. The three ways light interacts with a given medium and the relationship between them (transmission (T), reflectance (R), and absorptance (A)).[55]

The relationship shown above is important in identifying ways to determine thermal radiation behavior. For opaque materials in particular, transmission of light does not occur and, therefore, reflectance and absorptance, or emissivity, together sum to unity. The spectrum of wavelengths (Figure 4) shows that, for thermal radiation, the visible and near infrared regions are of particular interest. When attempting to understand heat transfer and the impact of material properties, it is key to explore the thermal and optical properties that govern transmission of heat.
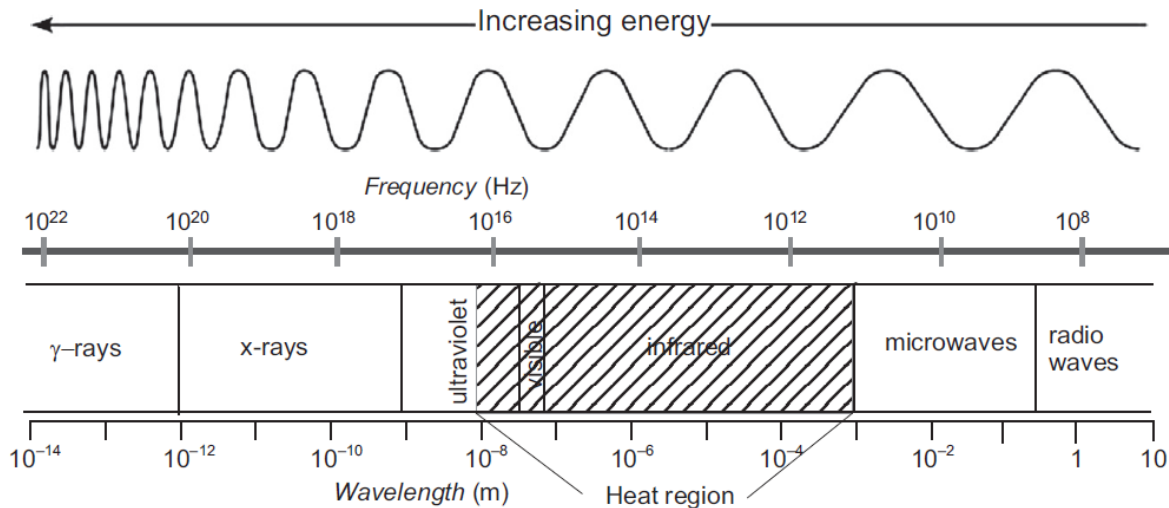
Figure 4. Spectrum of wavelengths for electromagnetic radiation showing heat emission present in the ultraviolet, visible, and the infrared.[54]

This report will focus on discussion of emissivity and the development of the capabilities to measure values for a range of temperatures. During this effort the emissivity as a function of temperature for several salts, as well as a couple of salt mixtures, was measured as a preliminary attempt to design an approach for accurate measurement of emissivity. The results of this initial effort are described below.

2. Experimental Configuration for Emissivity Measurement

The ideal experimental configuration for measuring emissivity will allow for the determination of values without interference from the surrounding furnace, the vessel, or gaseous phases that may be present. There are several approaches to measuring emissivity, the two considered in this work are briefly described here.

The first, and most direct, is the use of a pyrometer with the ability to internally determine emissivity. A pyrometer with an internal reference will adjust the emissivity value at a specific wavelength to provide the emissivity of the material being interrogated in a specified temperature range. The second approach is the measurement of the steady-state temperature of a system along with the apparent temperature of a material in said system, which are then related according to the Stefan-Boltzman law. The law says that the radiative energy transfer is proportional to a material's absolute temperature raised to the fourth power, scaled with the Stefan-Boltzman constant.[56] When the Stefan-Boltzman law is modified for a, diffuse graybody surface, the following equation is derived:

$$q = \varepsilon \sigma T^4 \tag{7}$$

where: q = the total emitted energy, ε = the emissivity value of the object, σ = the Stefan-Boltzman constant (5.67037 x 10^{-8} (W/(m^2·K^4)), and T = the absolute temperature of the surface (in K). A graphic of an experimental set up that could be used for either of the above approaches is shown below (Figure 5).
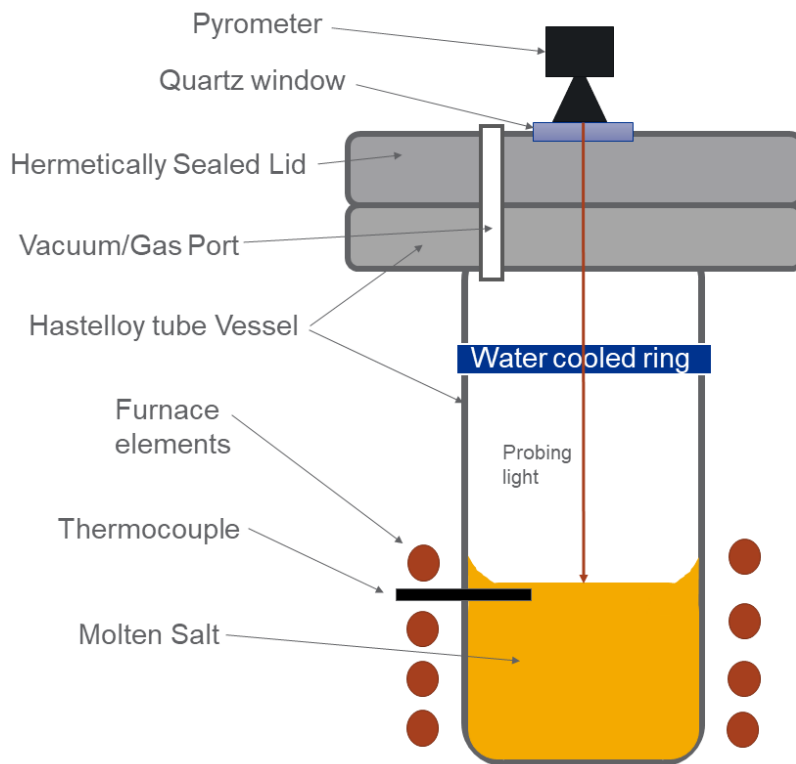
Figure 5. Proposed system for emissivity measurement of molten salts.

The pyrometer would remotely measure the salt batch and be protected from vapor by an optical window (shown as the quartz window in 5). The water-cooled ring can help condense vapors to maintain the integrity of the window and any components at the top end of the set up. The design above would allow for an inert atmosphere and variations in the vessel material used during testing. This facilitates the ability to not only control the salt environment but also determine potential impacts of salt-vessel interactions. This configuration could also be transferred to an area suitable for testing radiological materials including actinide-based salts.

3. Powders, Batching, and Characterization of Cl salts

The salt powders used in this study were high purity NaCl (99.999% metals basis) and KCl (99.999% metals basis) purchased from American Elements. These salts where opened, stored, and mixed in ambient atmospheres. Intermediate compositions were mixed in bulk batches, 25-50g, by hand with a mortar and pestle. Compositions are identified using the following notation: ClNaKxx(x)yy(y) in which xx(x) represents the mol% of NaCl from 0.0 to 100 percent and yy(y) represents the mol% of KCl from 0.0 to 100 percent. Therefore, the eutectic composition of 51 mol% NaCl - 49 mol% KCl would be labeled as ClNaK5149. Phase purity of the salts was confirmed with x-ray diffraction (XRD) (Figure 6) using a Rigaku Ultima IV with a Cu K-alpha source ($\lambda = 1.5406$ Å). Salt powders were scanned from 5 to 75° 2Ө with a 0.01° step size, a 2.0 second dwell, and a 10 mm variable divergent slit. The TOPAS v6 software package was used to determine diffraction patterns and identify crystals present. XRD analysis, indicates the presence of only NaCl and KCl crystals, indicating the salts are free of any major inclusion of secondary crystalline contaminants.
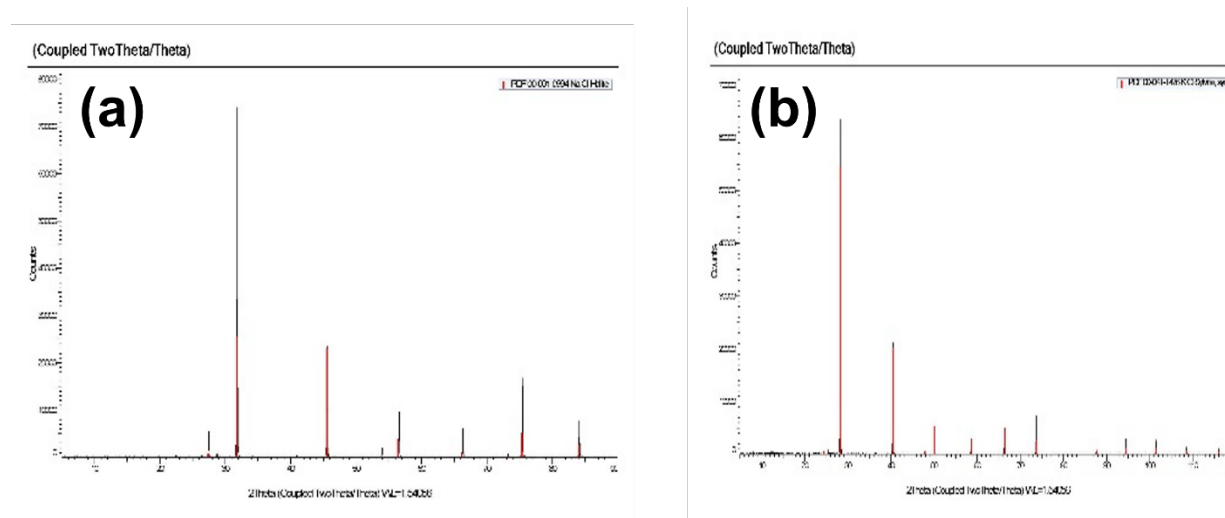
Figure 6. XRD analysis and peak fittings for the baseline (a) NaCl and (b) KCl powders used in this study.

Water quantification within the salt samples was achieved using Karl Fischer(KF) coulometric titrimetry (Photovolt Aquatest 2010) (Table 2). This methodology has been effectively applied in measuring moisture contents in a variety of liquid samples and has recently been extended to salt systems. Measurements on both pure KCl and NaCl indicate the presence of ~0.8 wt% H_2O. This result was somewhat surprising for salts that had been stored in ambient conditions for several years, as much larger water contamination was expected. Additionally, it's expected that water at measurement temperatures will be even less as isothermal holds above 500 °C should evaporate any remaining free water. Future experiments will investigate the effects of water content on the emissivity of the salts.

Table 2. Water detected in the salts as determined by KF titration.

Salt	Sample Mass (mg)	Water Mass (μg)	Water Concentration (Wt.%)
KCl	105.9	845.9	0.798
NaCl	139.3	1099.7	0.789

4. Determination of Surface Stability for Salts

To properly measure from above a molten salt, it is advantageous to ensure a still melt surface before measurements. Therefore, salts were prepared and imaged upon heating. An example graphic of how a material's surface can impact reflection of light of different wavelengths is shown in 7. A diffuse surface is desired for measuring the emissivity as some of the signal should return to the pyrometer even if the incident pyrometer beam is not perfectly perpendicular with the surface.
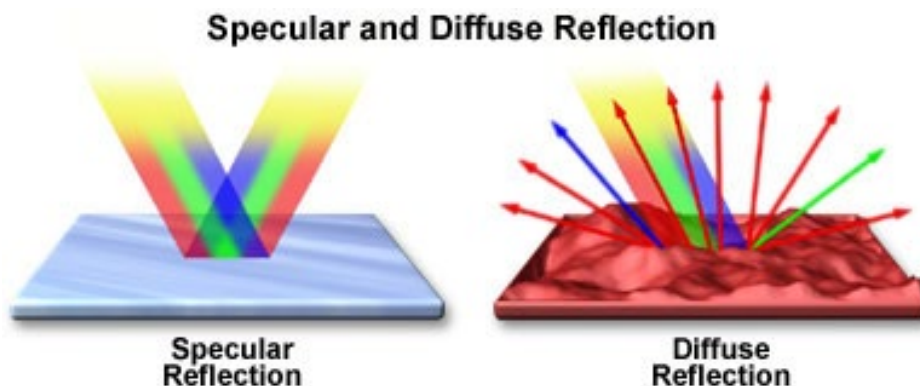
Figure 7. Specular reflection versus diffuse reflections.[1]

The first salt measured was ClNaK5149, the eutectic mixture for NaCl [51 mol%] and KCl [49 mol%]. A box furnace equipped with a cannon digital camera was used to image salts in a silica crucible (AdValue Tech) from room temperature to approximately 800 °C. The furnace and camera are shown in 8.
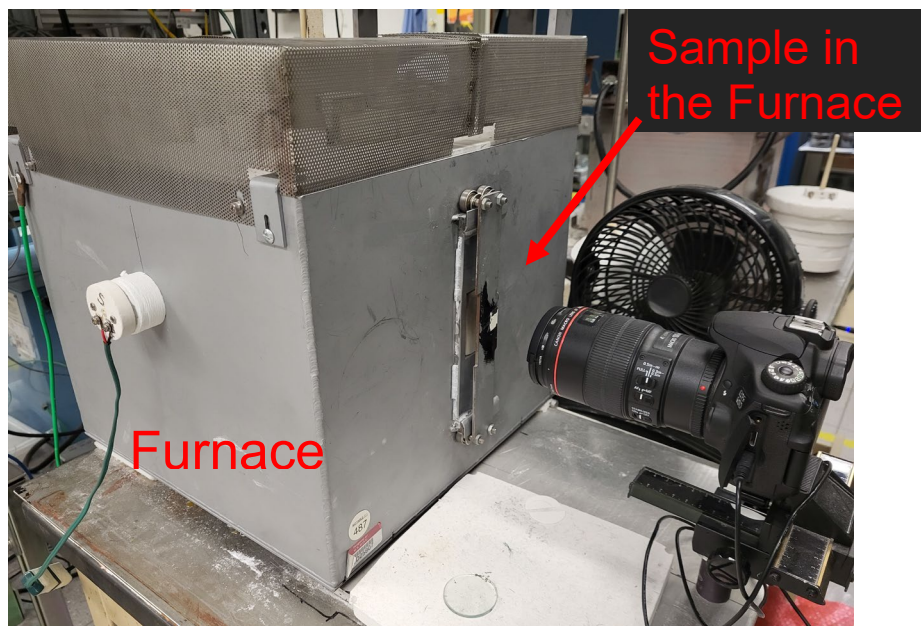
Figure 8. Furnace and camera setup used to image salts upon heating.

---

[1] Olympus-lifescience.com

These initial tests were conducted to understand the turbulence at the surface of salts upon heating. ClNaK5149 powders were heated from room temperature to 500, 600, and then 700 °C, at 10 °C/min with an isothermal hold for one hour at each temperature. Power to the furnace was turned off to allow cooling to room temperature (at approximately 12 °C/min). Images of the salt in the furnace at different temperatures, and after treatment, are shown in Figure 9.
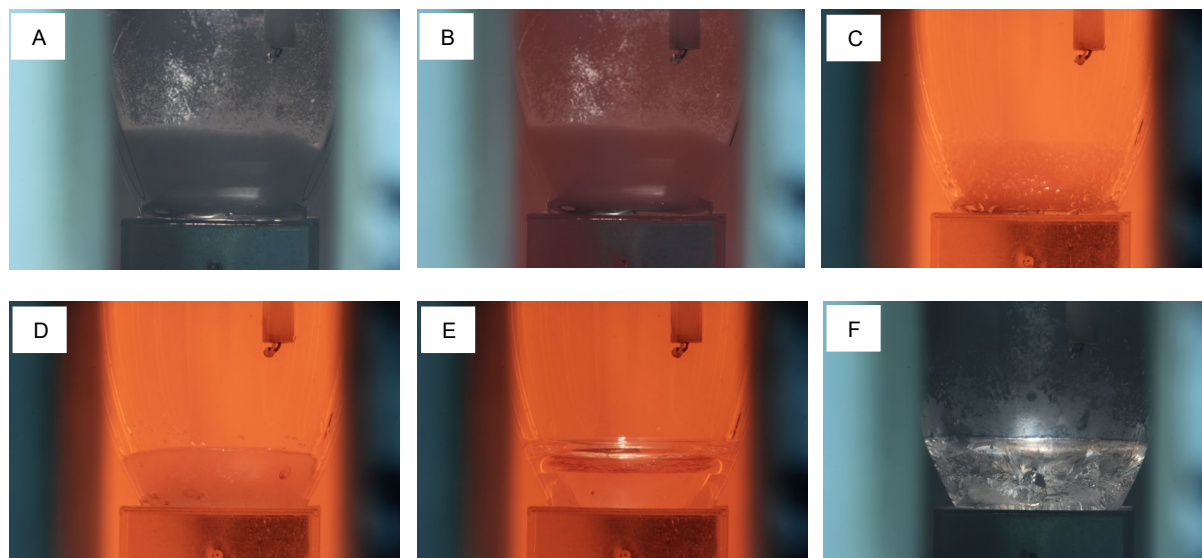
Figure 9. Picture of ClNaK5149 at A) room temperature, B) 500/600 °C, C) 700 °C at 1 min, D) 700 °C at 5 min, E) 700 °C at 10 min, and F) room temperature post-thermal cycling.

The testing showed that once the salt melts, and trapped air bubbles are released (as shown in 9-C), the salt surface is still (Figure 9-E). Generally, salts have lower viscosities, therefore air bubble release happens quickly and then the surface disturbance is minimal afterward. It was interesting to note that some discoloration was present, most likely impurities, which moved to the top of the melt with time (seen as a layer near the top 9-E). ClNaK5149 was remeasured in the same furnace but heated from room temperature to 1,000 °C at 10 °C/min. The salts produced from both the 700 °C and 1000 °C runs are shown below (Figure 10).
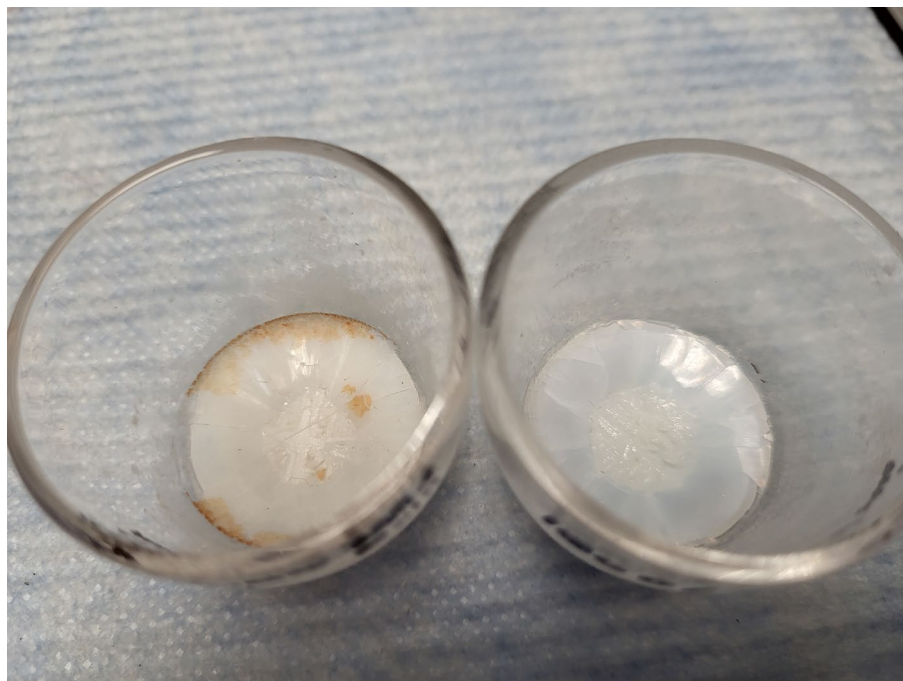
Figure 10. ClNaK5149 salt after the 700 °C (left) and 1000 °C heat treatments

The 700 °C sample shows some discoloration from unknown impurities that moved to the surface. These impurities are absent in the 1000 °C sample, likely due to burning off at the higher temperature. Further work should be done to explore what caused this discoloration.

5. Emissivity Measurements

As mentioned above, while there are many ways to determine emissivity, the ideal experimental configuration for measuring emissivity will allow for the determination of salt values without interference from the surrounding furnace, the vessel, or gaseous phases that may be present. The approaches attempted for measuring emissivity as part of this effort, characterization of the measured salt by XRD and Karl Fisher (KF) titration, as well as investigation of the NaCl-KCl system are discussed below.

5.1.   Proof of Concept Measurements

For temperatures above 500 °C, measurements were attempted in a Tilt-Pour induction melter with a copper coil. The system is equipped with a Williamson pyrometer (λ = 1.3 microns; field of view = 0.1 inches diameter cross section at 6 inches from the pyrometer) and samples were placed in a metal crucible to allow for coupling of the induction coil with a metal vessel. The salt and metal vessel were then placed inside an alumina crucible (AdValue Tech) as a secondary containment. The induction furnace with the Williamson optical pyrometer mounted above is shown below in Figure 11.
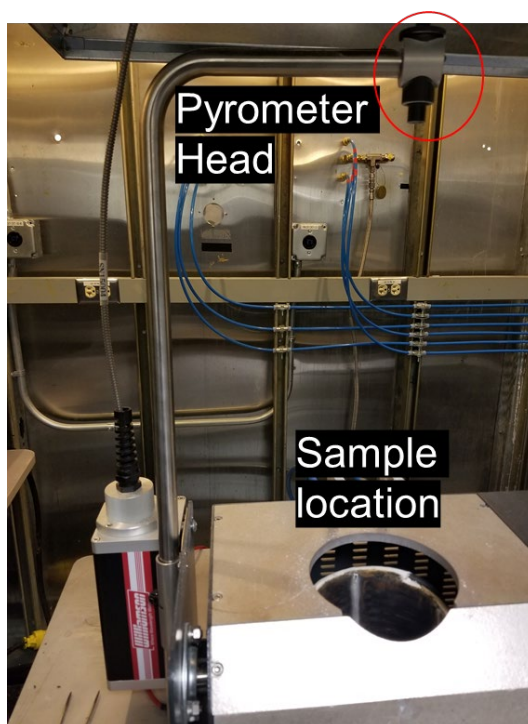
Figure 11. Induction coil furnace with optical pyrometer.

The Na-K-Cl eutectic and crucibles were used in the induction coil furnace and heated to approximately 850 °C. The pyrometer was aimed at the salt surface with an LED guide, as shown in the picture below (Figure 12). As the LED guide is larger than the laser incident area, it appears as if minimal interception of Ni crucible or other furnace signals were present.

Figure 12. Shows the size of the pyrometer LED size which should be much larger than the incident area of the pyrometer laser.

The system was set to 850 °C but the open-air configuration resulted in loss of heat and vapor. The sample heating and associated changes can be seen below (Figure 13). The resulting vapor is quite visible as the temperature increases. Indicating an increase in the vapor pressure of the salt with temperature. This confirms that the proposed hermetically sealed Ni vessel (5) would be an improved experimental configuration.

Figure 13. ClNaK5149 at 500 C (left) 700 C (middle) and 850 C (right).

The pyrometer was aimed at the surface and emissivity was determined despite the presence of vapor. The temperature on the pyrometer was automatically adjusted to match the temperature of the controller and when the temperatures matched an emissivity value was determined. The readings at various temperatures are shown below in Table 3.

Table 3. Initial emissivity measurement readings for molten ClNaK5149 salt.

Emissivity value	Controller Temperature	Single Wavelength Temperature
0.55	872	899
0.74	864	873
0.80	864	863

It was determined that the emissivity value for ClNaK5149 at ~850 °C is near 0.80. Validation of the initial measurement (λ=1.3 μm) was performed by comparison of the results to reflectance values from literature (2 μm to approximately 12 μm, taken at 680ºC.).[57] If we take the following Kirchhoff relation into account (Equation 8), we see that the emissivity value of 0.8 and the reflectance value, ~0.2, measured for 50 mol% NaCl – 50 mol% KCl do indeed sum to unity.

$$R_{diff,\lambda} + \varepsilon_\lambda = 1 \tag{8}$$

This is important because it implies our salts are opaque under the conditions tested. Indicating that the thickness of the salt tested was sufficient that no signal from the salt-nickle crucible interface was picked up in our measurments. Assuming the literature value is correct, this also imples that our postulated method and prototype device has correctly measured the emissivity of ClNaK5149 at ~850 °C.

If we take the measured thickness of our salt (measured before melt) as ~6.35 cm and set our absorptivity (0.8) equal to our emissivity (0.8) as defined by Kirchoff's law (Equation 5), we can then use Equation 6 to calculate the absorption coefficient of our ClNaK5149 salt. The resulting value is 25 m^{-1} which is significantly higher than that predicted by Challeff (5 m^{-1}) and near the upper value measured by Ewing et al. for FLiNaK.[51, 52] Going back to the model proposed by Challeff, and interpolating based on his results, we can safely assume that radiative heat transfer will contribute more than 20% of the total heat transfer in a HX at 800 °C based on the current measurements.

5.2.   Effects of Composition and Temperature

A systematic study was setup to investigate the effects of temperature and composition on the emissivity within the NaCl-KCl and NaF-LiF systems. The salts were placed in quartz crucibles (AdValue Tech) and placed in a Thermolyne muffle furnace using the Williamson pyrometer as described above (Section 5.1). Although NaF and LiF salts were not as extensively tested for purity as the Cl salts (Section 3) they did come from high purity stock (NaF (Sigma Aldrich, 99.0% metals basis), (LiF (Sigma Aldrich, 99.995% metals basis)). The Thermolyne furnace was chosen over the induction melter in the previous section for increased temperature control. Samples were placed into the furnace, and the guiding light of the pyrometer was used to center the beam on the salt. A picture of the guiding beam on a sample is shown below (Figure 14). After ensuring the pyrometer was aimed at the center of the salts in the crucibles, the samples were measured at 100 °C increments from 550 to 850 °C for the NaCl-KCl salts. For the NaF LiF salts the samples were measured in 200 °C increments from 600 to 1000 °C. The change in temperatures tested was to ensure capturing of emissivity before and after melting for each

composition. The furnace was heated empty and when the desired temperature was reached, the salts were placed inside and allowed to equilibrate for 30 min to 1 hour (particularly at temperatures above the known m.p.).

Figure 14: Guiding light from the pyrometer on ClNaK5149 in the muffle furnace at 550 °C. Note the use of larger crucibles and the crucibles closer to the pyrometer in this second study, ensuring the guide light (i.e. laser) is well within the crucible and not capturing signal from the crucible wall.

Figure 15 shows the measured emissivity results for pure NaCl, KCl, and the ClNaK5149 (eutectic) compositions. Averaged emissivity values ranged from 0.9 at 550 °C and decreased to 0.78 at 850 °C. This represented a significant decrease with each 100 °C temperature step, in which the measured emissivity was outside of the error bars of the subsequent step. The overall trend was plotted with a second order polynomial fit (Equation 9) with an R^2 value of 0.98. Surprisingly, there was no observed change in trends between salts measured at solid and molten state.

$$\varepsilon = 1E^{-6}T^2\text{-}0.0018T\text{+}1.5735 \tag{9}$$

Although there was not a significant change in emissivity values for different NaCl-KCl chemistries at the same temperature (from 550 to 750 °C), the eutectic composition showed an increase in emissivity of ~0.3 from the two endpoints at 850 °C. Future work will be performed to repeat this measurement with newly synthesized salts to ensure it's not an outlier due to contamination or improper experimental setup. If it holds, it could be an indication of a more complex dimer formation resulting in significant altered vibrational bands and emission spectra.
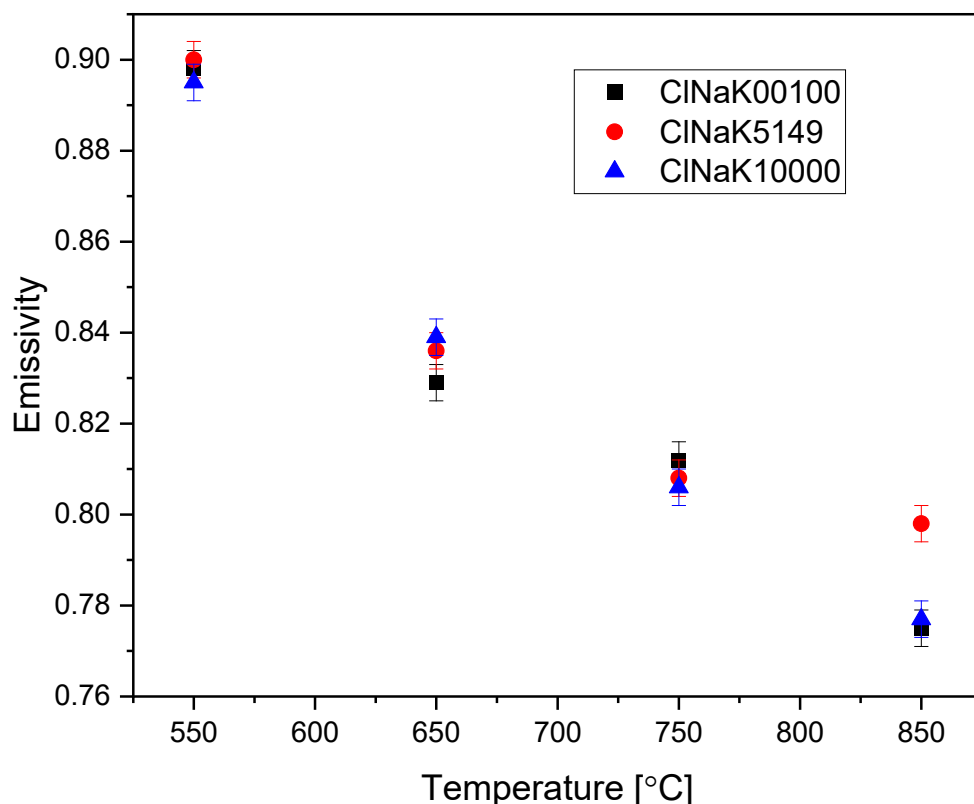
Figure 15. Measured emissivity for ClNaK salts from pure NaCl to KCl from 550 to 850 °C.

Figure 16 shows the emissivity results for pure NaF, LiF, and the FliNa6139 (eutectic) compositions. Average emissivity values ranged from ~0.850 at 600 °C and decreased to ~0.839 at 1000 °C. Although this represented an overall decrease, some temperature steps actually exhibit an increase. For instance, FLiNa6139 shows an increase of 0.004 between 600 and 800 °C but that may be within the sensitivity of the pyrometer. It is not known at this point the cause for the differences in behavior between the two systems. Future work will involve at least triplicate measurements at each temperature to develop a better understanding of measurement error and uncertainty. Similar to ClNak5149, FLiNa6139 (the mixed salts) exhibits a large increase in emissivity after 800 °C. As postulated before, this could be a sign of more complex dimer formation at higher temperatures.

Overall, the fluoride salts exhibit a higher emissivity at a given temperature than the chloride salts. This could be due to the higher bond dissociation energies of the F salts as compared to the Cl salts (Table 4).[58] In other words, the higher the bond energy and the more light (i.e. energy) is absorbed/emitted in the salt at the 1.3 μm wavelength tested. This can also be seen within the FLiNa system as the pure LiF shows a pronounced increase in emissivity compared to pure NaF, especially at sub melt temperatures. Future work will continue to elucidate the impact of bond strength as well as ionic structure on optical properties.
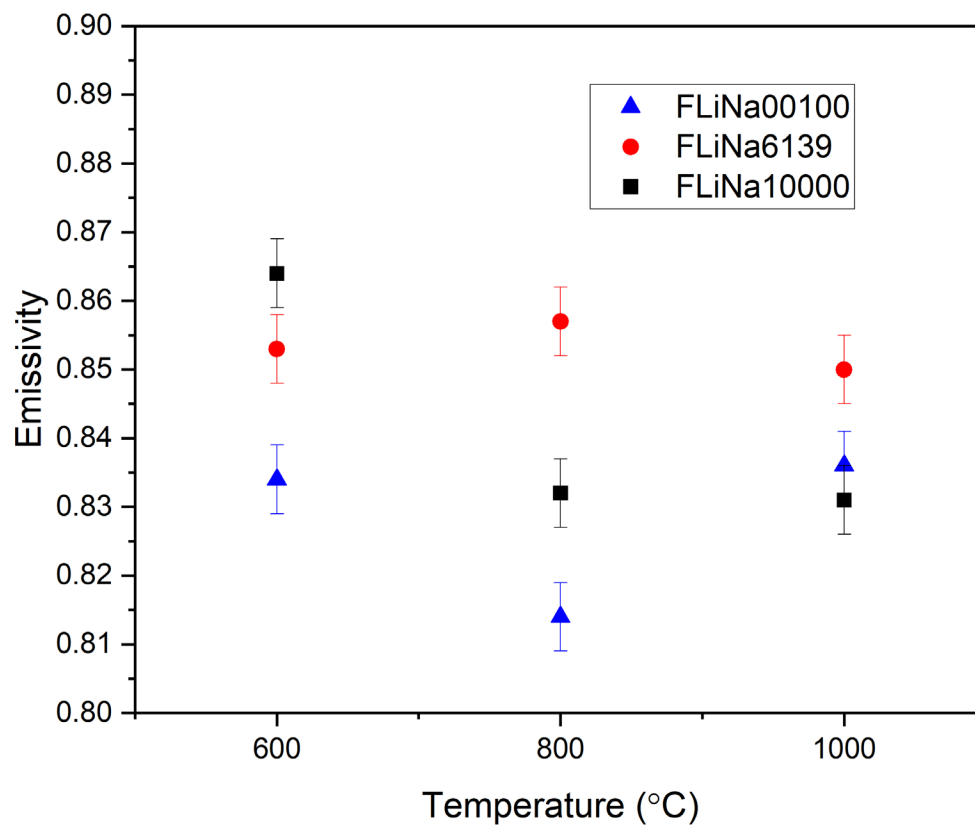
Figure 16. Measured emissivity for FLiNa salts from pure NaF to LiF from 600 to 1000 °C.

Table 4. Bond Dissociation Energy of the single salts.[58]

Compound	D^o_{298} (KJ/mol)
NaCl	412.1
KCl	433
LiF	577
NaF	477.3

6. Future Work

6.1. Experimental Path Forward

An inert, system design capable of measuring emissivity of radiological salts will be developed to via optical pyrometer in conditions relevant to reactor operation. An inert glovebox is under final installation and will be available in FY23 (Figure 17). This will allow for storage, mixing, and loading of actinide salts in an inert environment and will allow for work on planned actinide bearing systems. A tube furnace (Figure 18a) has been identified to house the inert system containment vessel capable of 1200 °C. Nickel tube and plating has been purchased to fabricate an inert system containment vessel similar to that shown (Figure 18b). This vessel will include a sealable lid with o-ring outside the furnace and a window for remote measuring of the salt temperature/emissivity values, as well as ports for flushing the system with the desired gas. This will allow for stabilization of the vapor (seen coming off the slats in Figure 13) within the head space above the molten salts ensuring the composition is stable after an isothermal hold. This sealable system will also allow for testing of fuel salts, ensuring the encapsulation of actinide components that have become volatile. Finally, vacuum or an inert atmosphere will be applied to limit reaction with oxygen(O_2) or moisture (H_2O). The inert glove box will also allow for loading and removal of salts within an inert atmosphere ensuring fundamental properties can be tested on anhydrous salts.

Figure 17. Inert radiological glove box for storage, mixing, and loading of hydroscopic coolant and fuel salts.
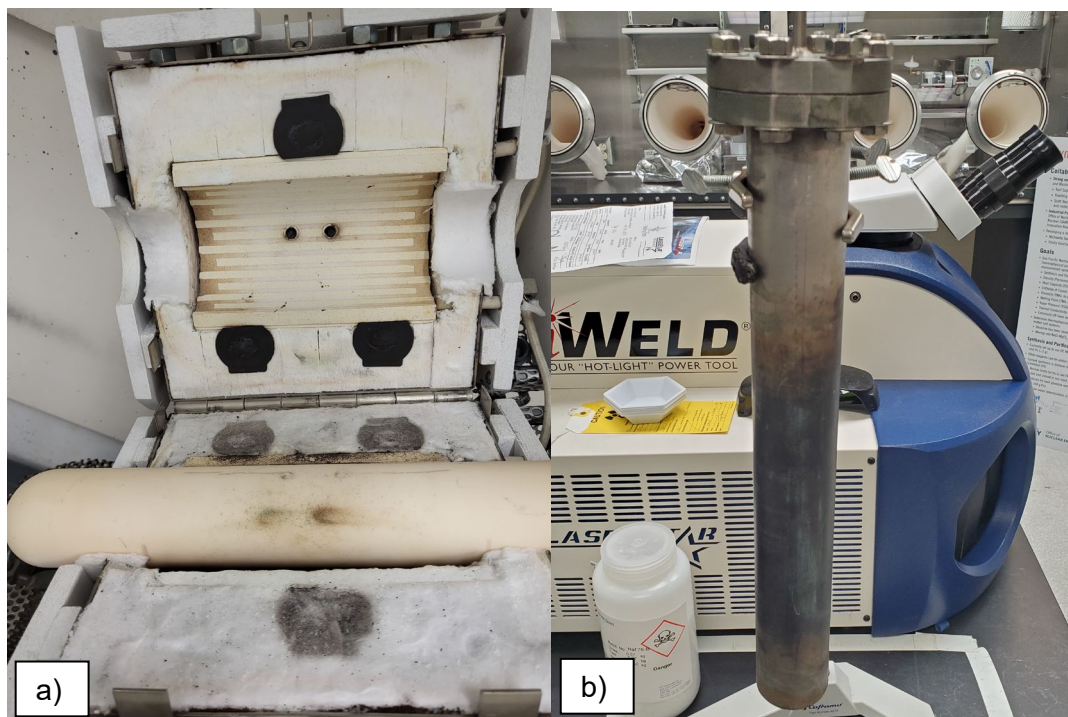
Figure 18. a) Tube furnace for high temperature hermetically sealed salt measurement system and b) Ni crucible for testing of both hydroscopic and actinide bearing salts under a hermetically sealed inert atmosphere.

A pyrofiber Lab 1550 Optical Emissivity Measuring Infrared Thermometer has been purchased and will be installed for future experimentation. This unit can perform measurements at temperatures from ~275-1000 °C. Additionally, measurements at various temperatures will be attempted at a wide range of wavelengths with an FTIR; reproducing the reflectance data that was used to verify the emissivity results as well as verifying that salts are truly opaque.

Future work is planned for both coolant and fuel salts in the Cl and F salt systems. Specifically, the $NaCl-KCl-MgCl_2$ and $LiF-NaF-BeF_2$ coolant systems as well as the $UCl_4(F)-ThCl_4(F)-PuCl_4(F)$ system is of interest. This work will start with single salt and binary systems and move towards more complex ternary and quaternary systems. A more detailed roadmap for thermal property measurements can be found in ORNL report ORNL/SPR-2020/1865.[34]

6.2. Programmatic Vision

There is also a PNNL vision of determining the total thermal conductivity of the salt and breaking it down into its molecular and radiative components. Total thermal conductivity will be calculated with measurements of thermal diffusivity (D), heat capacity (C_p), and density (ρ) using Equation 10.

$$\kappa_t = DC_p\rho \tag{10}$$

Thermal diffusivity measurements of molten salts will be measured using a laser flash system. Custom crucibles are in development for the molten salts. A laser welding encapsulation technique has been developed to produce high accuracy heat capacity measurements through drop calorimetry. Density measurements, in good agreement with literature, have been established using a pycnometry/geometrical approach. Coupled with emissivity measurements, the radiative and molecular portions of the thermal conductivity with temperature and composition can be determined. The goal of this work is to elucidate the fundamental physics behind heat transfer in molten salts and determine compositions of enhanced thermal conductivity. Systematic studies are planned for additions of H_2O, Cr, Fe, and Ni to understand the effects of salt impurities and corrosion on chemistry and structure and its resulting impact on molecular and radiative thermal transport within molten salts.

7. Summary

The ability to measure heat transfer properties such as emissivity are of high importance because the proposed operating systems of Gen-IV MSR are entering a regime in which radiative heat transfer is significant. Although not given as much attention as other thermophysical properties, it was shown through fundamental heat transfer calculations, previous work found in the literature, and the use of the scant available measured optical properties, that radiative transfer could contribute over 20% of the total thermal flux within a heat exchanger system. By understanding the nature of radiative heat transfer and the properties that control it, designers can utilize these effects for increased efficiency in MSR systems. Failure to understand or measure these properties could result in significant parasitic losses and heat soak to vital components.

The focus of this report was ultimately to detail progress on the development of a novel emissivity measurement capability. This was ultimately successful, as shown with the inclusion of two preliminary data sets on a Cl and F salt system. The development started with a simple conceptual design based off the Stefan-Bolzmann Law (Figure 4), followed by the construction of a prototype test apparatus, and validation through the measurement of emissivity values that agree with available literature. Measured emissivity values for the NaCl-KCl system ranged from ~0.9 to 0.77 from 550 to 850 °C, exhibiting relative compositional invariance but strong temperature dependence. Measured emissivity values for the NaF-LiF system range from 0.850 to 0.839 from 600 to 1000 °C, exhibiting strong compositional dependence and weaker temperature dependence. The fundamental nature of the general decrease in emissivity with temperature is currently unknown but future work is underway to elucidate the mechanics behind the measured properties.

In both systems, temperatures above 800 °C saw a shift upwards in emissivity values of the eutectic salts. This may be due to the formation of more complex dimer structures in the salts at these elevated temperatures. It was shown that the F-based salts had higher emissivity values across the system than the Cl salts at a given temperature. An initial hypothesis as to this trend was attributed to bond energy, in which higher bond energies lead to higher absorption and emission of light (energy). These two systems are of fundamental importance as they represent the building block to more complex understanding of the fundamental optical and radiative heat transport properties of coolant and fuel salts.

An experimental path forward was proposed that will involve the construction of an enclosed system with variable environmental conditions for testing of Cl, F, actinide salts with impurities and corrosion products from 275 to 1000 °C. This is part of the larger goal to measure the total thermal conductivity and the breakdown of the molecular and radiative parts of heat transfer and, ultimately, identifying salt compositions with improved heat transfer properties.

8. References

1. Abram, T. and S. Ion, *Generation-IV nuclear power (A review of the state of the science).* Energy Policy, 2008(36): p. 4323-4330.
2. *Review of Generation IV Nuclear Energy Systems* 2015, Institut de Radioprotection et de Surete Nucleaire France.
3. Kelly Beiershmitt, et al., *Basic Research Needs for Future Nuclear Energy: Report of the Basic Energy Sciences Workshop for Future Nuclear Energy.* 2017, United States office of Science: United States.
4. Williams, D.F. and P.F. Britt, *Molten Salt Chemistry Workshop: Innovative Approaches to Accelerate Molten Salt Reactor Development and Deployment.* 2017, Office of Nuclear Energy.
5. LeBlanc, D., *Molten salt reactors (A new beginning for an old idea).* Nuclear Engineering and Design, 2010. **240**: p. 1644-1656.
6. *Climate Change and Nuclear Power* 2018, International Atomic Energy Agency.
7. *Energy, Electricity and Nuclear Power Estimates for the Period up to 2050.* 2020, International Atomic Energy Agency.
8. W.B. Cottrell, et al., *Operation of the Aircraft Reactor Experiment* 1955, Oak Ridge National Laboratory, United States Atomic Energy Commission Tennessee.
9. Grimes, W.R., *Molten-Salt Reactor Chemistry.* Nuclear Applications & Technology, 1969. **8**: p. 137-155.
10. P.N. Haubenreich and J.R. Engel, *Experience with the molten-salt reactor experiment.* Nuclear Applications & Technology 1969. **8**: p. 118-136.
11. Serp, J., et al., *The molten salt reactor (MSR) in generation IV: Overview and perspectives.* Progress in Nuclear Energy, 2014. **77**: p. 308-319.
12. *Introduction*, in *Molten Salt Reactors and Thorium Energy*, T.J. Dolan, Editor. 2017, Woodhead Publishing. p. 1-12.
13. Forsberg, C.W. *An Advanced Molten Salt Reactor Using High-Temperature Reactor Technology* in *International Congress on Advances in Nuclear Power Plants* 2004. Pittsburgh, Pennsylvania.
14. S.M.A. Ibrahim, M.M.A. Ibrahim, and S.I. Attia, *The Impact of Climate Changes on the Thermal Performance of a Proposed Pressurized Water Reactor: Nuclear-Power Plant.* International Journal of Nuclear Energy, 2014: p. 1-7.
15. *2020 Annual Report*. 2020, Gen IV Internaltional Forum.
16. Saraf, N., et al., *Molten Salt Reactors and Their Development Ocer the Years - A Review.* International Journal of Mechanical and Production Engineering Research and Evelopment, 2018. **8**(3): p. 175-182.
17. Zheng, G., et al., *Thorium-based molten salt SMR as the nuclear technology pathway from a market-oriented perspective* Annals of Nuclear Energy, 2018. **116**: p. 177-186.
18. Mignacca, B. and G. Locatelli, *Economics and finance of Molten Salt Reactors* Progress in Nuclear Energy, 2020. **129**: p. 103503.
19. Zhou, J., et al., *Influence of 7Li enrichment on Th-U fuel breeding performace for molten salt reactors under differnt neutron spectra.* Progress in Nuclear Energy, 2020. **120**: p. 103213.
20. G.F. Flanagan, D.E. holcomb, and I. W.P. Poore, *MSR Fuel Qualification Considerations and Challenges.* 2018, Oak Ridge National Laboratory.
21. Nuttin, A., et al., *Potential of thorium molten salt reactors: Detailed calculations and concept evolution with a view to large scale energy production.* Progress in Nuclear Energy, 2005. **46**(1): p. 77-99.

22. Brun, C.L., *Molten salts and nuclear energy production.* Journal of Nuclear Materials, 2007. **360**: p. 1-5.

23. Benes, O. and R.J.M. Konings, *Molten Salt Rector Fuel and Coolant*, in *Comprehensive Nuclear Materials*. 2012. p. 359-389.

24. Boyd, S. and C. Taylor, *Chemical fundamentals and applications of molten salts*. 2017, Woodhead. p. 1-63.

25. Volkovich, V.A., et al., *Reactions and special of techetium and rhenium in chloride melts: a spectroscopy study.* Physical Chemistry Chemical Physics, 2002. **4**: p. 5733-5760.

26. P. Masset, *Iodide-based electrolytes: A promosing alternative for thermal batteries.* Journal of Power Sources, 2006. **160**: p. 688-697.

27. Masset, P. and R.A. Guidotti, *Thermal activated (thermal) battery technology Part II. Molten salt electrolytes* Journal of Power Sources, 2007. **164**: p. 397-414.

28. Bradshaw, R.W. and N.P. Siegel. *Molten Nitrate Salt Development for Thermal Energy Storage in Parabolic Trough Solar Power Systems*. in *Energy Sustainability*. 2008. Jacksonville, Florida: Sandia National Laboratories.

29. Shankar, A.R. and U.K. Mudali, *Corrosion of type 316L stainless steel in molten LiCl-KCl salt.* Materials and Corrosion 2008. **59**(11): p. 878-882.

30. Bradshaw, R.W., *Effect of Composition on the density of multi-component molten nitrate salts* 2009: Albuquerque, New Mexico.

31. Sridharan, K., *Thermal Properties of LiCL-KCl Molten Salt for Nuclear Waste Separation*. 2012, University of Wisconsin
Idaho National Laboratory.

32. Li, P., et al., *Thermal and Transport Properties of NaCl-KCl-ZnCl$_2$ Eutectic Salts for New Generation High-Temperature Heat-Transfer Fluids.* Journal of Solar Energy Engineering, 2016. **138**: p. 054501-1-8.

33. Xu, X., et al., *Experimental Test of Properties of KCl-MgCl$_2$ Eutectic Molten Salt for Heat Transfer and Thermal Storage Fluid in Concentrated Solar Power Systems.* Journal of Solar Energy Engineering, 2018. **140**: p. 051011-1-9.

34. J. McMurray, et al., *Roadmap for thermal property measurements of molten salt reactor systems* 2021, Oak Ridge National Laboratory.

35. Chase, M.W., *NIST-JANAF Thermochemical Tables, Fourth Edition.* Journal of Physical Chemical Reference Data, Monograph 9 1998: p. 1-1951.

36. P.D. Myers, J. and D.y. Goswami, *Thermal energy storage using chloride salts and their eutectics.* Applied Thermal Engineering, 2016. **109**: p. 889-900.

37. Ch.D. Chliatzou, M.J. Assael, and K.D. Antoniadis, *Reference Correlations for the Thermal Conductivity of 13 Inorganic Molten Salts* Journal of Physical and Chemical Reference Data, 2018. **47**: p. 033104.

38. S.S. Parker, et al., *Thermophysical properties of liquid chlorides from 600 to 1600K: Melt point, enthalpy of fusion, and volumetric expansion.* Journal of Molecular Liquids, 2022. **346**: p. 118147.

39. G.J. Janz, et al., *Molten Salts: Volume 4, Part 2, Chlorides and Mixtures: Electrical Conductance, Density, Viscosity, and Surface Tension Data.* Journal of Physical and Chemical Reference Data, 1975. **4**: p. 871-1178.

40. T. Bauer and W. Ding, *SFERA II Project Deliverable D15.4: Report on innovateive techniques for molten salts high temperature measurements* 2018, German Aerospace Center (DLR). p. 1-20.

41. W.T. Barrett and W.E. Wallace, *Studies of NaCl-KCl Solid Solutions. I. Heats of Formation, Lattice Spacings, Densities, Schottky Defects and Mutual Solubilities.* Journal of the American Ceramic Society 1954. **76**(2): p. 366-369.

42. D.S. Coleman and P.D.A. Lacy, *The phase equilibrium diagram for the KCl-NaCl system.* Materials Research Bulletin, 1967. **2**(10): p. 935-938.

43. D. Sergeev, K. Kobertz, and M. Muller, *Thermodynamics of the NaCl-KCl system.* Thermochimica Acta, 2015: p. 25-33.
44. J.C. Gomez and R. Tirawat, *Corrosion of alloys in a chloride molten salt (NaCL-LiCl) for solar thermal technologies.* Solar Energy Materials & Solar Cells, 2015.
45. Williams, D.F., *Assessment of candidate molten salt coolants for the NGNP/NHI Heat-Transfer Loop.* 2006, Oak Ridge National Laboratory
46. X. Xu, et al., *Basic properties of eutectic chloride salts NaCl-KCl-ZnCl2 and NaCl-KCL-MgCl2 as HTFs and thermal storage media measured using simultaneous DSC-TGA.* Solar Energy 2018. **162**: p. 431-441.
47. E.S. Scooby, et al., *Measurements of the liquidus surface and solidus transitions of the NaCl-UCl3 and NaCl-UCl3-CeCl3 phase diagrams.* Journal of Nuclear Materials 2015. **466**: p. 280-285.
48. Lewis, E.E., *Fundamentals of Nuclear Reactor Physics.* 2008: Academic Press.
49. Breeze, P., *Nuclear Power.* 2016: Academic Press.
50. P.V Bockh and T. Wetzel, *Heat Transer Basics and Practice.* 2012: Springer.
51. C.T. Ewing, J.R. Spann, and R.R. Miller, *Radiant Transfer of Heat in Molten Inorganic Compounds at High Temperatures.* Journal of Chemical and Engineering Data, 1961: p. 246-250.
52. Chaleff, E.S., *The Radiative Heat Transfer Properties of Molten Salts and Their Relevance to the Design of Advanced Reactors.* 2016, Ohio State University.
53. H. Watanabe, et al., *Spectral Emissivity Measurements* in *Experimental Methods in the Physical Sciences.* 2014. p. 333-366.
54. C. Meola, S. Boccardi, and G.M. Carlomagno, *Infrared Thermography in the Evaluation of Aerospace Composite Materials (Infrared Thermography to Composites).* 2017, Woodhead Publishing.
55. K.D. Dahm and D.J. Dahm, *Principles of DIffuse Reflectance Spectroscopy*, in *Handbook of Near-Infrared Analysis.* 2021, CRC Press.
56. J.J. Derby and A. Yeckel, *Heat Transfer Analysis and Design for Bulk Crystal Growth: Perspectives on the Bridgman Method*, in *Handbook of Crystal Growth*, T. Nishinga, Editor. 2015, Elsevier.
57. P.D. Myers, J., D. Yogi Goswami, and E. Stefanakos, *Molten Salt Spectroscopy for Quantification of Radiative Absorption in Novel Metal Chloride-Enhanced Thermal Sotrage Media.* Journal of Solar Energy Engineering, 2015. **137**: p. 041002.
58. Luo, Y.R., *Comprehensive Handbook of Chemical Bond Energies.* 2007, Boca Raton, Fl: CRC Press.

Pacific Northwest
National Laboratory

902 Battelle Boulevard
P.O. Box 999
Richland, WA 99354

1-888-375-PNNL (7665)

www.pnnl.gov